Biochimica et Biophysica Acta 1838 (2014) 482–492

Contents lists available at ScienceDirect

Biochimica et Biophysica Acta

journal homepage: www.elsevier.com/locate/bbamem

Insertion of apoLp-III into a lipid monolayer is more favorable for saturated, more ordered, acyl-chains

Sewwandi S. Rathnayake [a], Mona Mirheydari [b], Adam Schulte [a], James E. Gillahan [a], Taylor Gentit [a], Ashley N. Phillips [a], Rose K. Okonkwo [a], Koert N.J. Burger [c,1], Elizabeth K. Mann [b], David Vaknin [d], Wei Bu [d,2], Dena Mae Agra-Kooijman [b], Edgar E. Kooijman [a,*]

[a] Department of Biological Sciences, Kent State University, Kent, OH 44242, USA
[b] Physics Department, Kent State University, Kent, OH 44242, USA
[c] Endocrinology and Metabolism, Faculty of Science, and Institute of Biomembranes, Utrecht University, Utrecht The Netherlands
[d] Ames Laboratory and Department of Physics and Astronomy, Iowa State University, Ames, IA 50011, USA

ARTICLE INFO

Article history:
Received 10 August 2013
Received in revised form 20 September 2013
Accepted 25 September 2013
Available online 4 October 2013

Keywords:
Exchangeable apolipoprotein
Diacylglycerol
Langmuir monolayer
X-ray reflectivity and diffraction
Insertion isotherm
Protein–lipid interaction

ABSTRACT

Neutral lipid transport in mammals is complicated involving many types of apolipoprotein. The exchangeable apolipoproteins mediate the transfer of hydrophobic lipids between tissues and particles, and bind to cell surface receptors. Amphipathic α-helices form a common structural motif that facilitates their lipid binding and exchangeability. ApoLp-III, the only exchangeable apolipoprotein found in insects, is a model amphipathic α-helix bundle protein and its three dimensional structure and function mimics that of the mammalian proteins apoE and apoAI. Even the intracellular exchangeable lipid droplet protein TIP47/perilipin 3 contains an α-helix bundle domain with high structural similarity to that of apoE and apoLp-III. Here, we investigated the interaction of apoLp-III from *Locusta migratoria* with lipid monolayers. Consistent with earlier work we find that insertion of apoLp-III into fluid lipid monolayers is highest for diacylglycerol. We observe a preference for saturated and more highly ordered lipids, suggesting a new mode of interaction for amphipathic α-helix bundles. X-ray reflectivity shows that apoLp-III unfolds at a hydrophobic interface and flexible loops connecting the amphipathic α-helices stay in solution. X-ray diffraction indicates that apoLp-III insertion into diacylglycerol monolayers induces additional ordering of saturated acyl-chains. These results thus shed important new insight into the protein–lipid interactions of a model exchangeable apolipoprotein with significant implications for its mammalian counterparts.

1. Introduction

Neutral lipids (e.g. triacylglycerols and cholesterolesters) need to be packaged in order to exist in stable form in solution. In the blood stream as well as inside cells this packaging is mediated by a phospholipid–protein monolayer. The protein component consists of both intrinsically associated and exchangeable proteins. Protein–lipid interactions for exchangeable proteins are critical for their reversible interaction with the neutral lipid particle (lipoprotein in the case of transport) [1]. Lipoprotein particles in both mammals and insects have similar structures and functions, including intrinsically associated proteins (so-called non-exchangeable apolipoproteins) that provide structural integrity. Mammalian lipid transport is complex and involves distinct types of particles and many different kinds of apolipoproteins. Compared with mammalian lipid transport, insect hemolymph carries neutral lipids in a single type of lipoprotein called lipophorin (HDLp). The non-exchangeable apolipoproteins, apolipophorinI (apoLp-I) and apolipophorinII (apoLp-II) (homologues of mammalian apoB100), form an integral part of the structure of lipophorin. Aside from apoLp-I and apoLp-II some insects also have a single exchangeable apolipoprotein, apolipophorinIII (apoLp-III). This low molecular weight (18–20 kD) exchangeable apolipoprotein associates with lipophorins in the hemolymph, facilitating the delivery of neutral lipids into the insect flight muscle during flight (for recent reviews: [2–4]).The structure and function of apoLp-III is similar to that of mammalian proteins apoE and TIP47/perilipin 3 [5–7]. ApoLp-III can reversibly associate with the lipophorin particle existing in both lipid-bound and lipid-free forms depending on the status of lipid metabolism in the insect body [8,9]. The incorporation of ApoLp-III molecules to growing lipophorin particles (called LDLp after acquiring additional lipid and apoLp-III) is thought to stabilize them [9–11].

In contrast, mammals contain many different types of exchangeable apolipoproteins, such as apoE, apoA-I, apoA-II, apoC-I, apoC-II and apoC-III [12]. Apolp-III from insects shares many of the characteristics of the mammalian exchangeable apolipoproteins, as all possess

* Corresponding author. Tel.: +1 330 672 7967; fax: +1 330 672 2959.
E-mail address: ekooijma@kent.edu (E.E. Kooijman).
[1] Currently at the Dutch Order of Medical Specialists, Utrecht, the Netherlands.
[2] Currently at Advanced Photon Source, Argonne National Laboratories, Argonne, IL, USA.

0005-2736/$ – see front matter © 2013 Elsevier B.V. All rights reserved.
http://dx.doi.org/10.1016/j.bbamem.2013.09.020

amphipathic α-helices that are involved in lipid binding [13]. The monomeric lipid-free state of apoLp-III circulates in the hemolymph of a resting insect until it associates with the expanding lipophorins during insect flight to supply fuel to the flight muscle tissue by delivering neutral lipids from the fat body [11].

ApoLp-III from the migratory locust *Locusta migratoria* and the tobacco hornworm *Manduca sexta* (two evolutionarily divergent species) is commonly used as model apolipoprotein (see e.g. [2,3,14]). Both are found in high concentrations in the hemolymph of adults in both species [15–17]. Despite the low sequence similarity between these two apolipoproteins, they share a great degree of structural and functional similarity [2,3]. A similar degree of structural and functional similarity exists between apoLp-III and the N-terminus of the mammalian apolipoprotein apoE and the C-terminus of the mammalian lipid droplet binding protein TIP47/perilipin 3 [6,7].We use apoLp-III from *L. migratoria* as model apolipoprotein to investigate the interaction of an amphipathic α-helix bundle protein with (phospho-) lipid monolayers.

There are few reports in the literature detailing the fatty acid composition of insect lipophorin [18,19]. What has been published suggests that fatty acids with chains of 16 and 18 carbons are most common in the core and the phospholipid monolayer appears to be enriched in 18:0, 18:2, and 18:3 fatty acids [19]. However the exact lipid composition is unknown. ApoLp-III interacts preferentially with diacylglycerols (DAGs) and to a lesser degree with phospholipids [20,21]. Since most insect lipophorin is rich in DAG and other hydrocarbons and phospholipids [22,23], this preference for DAG appears to make sense. On the other hand, mammalian lipoproteins contain a core of non-polar lipids including triacylglycerols (TAGs) and cholesterol esters, and are covered by a monolayer of phospholipids and cholesterol interspersed with apolipoproteins [12]. Whether the binding of apoLp-III to lipophorin is facilitated by actual chemical recognition (as in the case of an enzyme and substrate) of DAG or is due to physical properties of the lipid monolayer is unclear and has not been investigated in great detail. The objective of this work is to delineate the specific interactions required for apoLp-III phospholipid interaction. Our choice of lipids spans the range of lipids found in insect lipophorin. In addition to detailed insertion isotherms, we use surface sensitive x-ray reflectivity and x-ray diffraction to further investigate the nature of protein–lipid interaction. In order to most closely mimic the in vivo conditions we used native apoLp-III isolated from *L. migratoria*.

1.1. Materials and methods

POG (1-palmitoyl-2-oleoyl-*sn*-glycerol), POPC (1-palmitoyl-2-oleoyl-*sn*-glycero-3-phosphocholine), POPE (1-palmitoyl-2-oleoyl-*sn*-glycero-3-phosphoethanolamine), POPG (1-palmitoyl-2-oleoyl-*sn*-glycero-3-phospho-(1′-rac-glycerol), DOG (1,2-dioleoyl-*sn*-glycerol), DOPC (1,2-dioleoyl-*sn*-glycero-3-phosphocholine), DOPE (1,2-dioleoyl-*sn*-glycero-3-phosphoethanolamine), and DOPG (1,2-dioleoyl-sn-glycero-3-phospho-(1′-rac-glycerol) were purchased from Avanti Polar Lipids (Alabaster, AL). All the lipids were purchased in powdered form except for POG and DOG which were dissolved in chloroform. All lipids were used without further purification. Powdered lipids were dissolved in a 2:1 (v/v) mixture of chloroform and methanol. ApoLp-IIIb from *L. migratoria* was obtained and purified from insects or expressed as recombinant protein as previously described [24,25]. All other chemicals used were at least 99.8% pure (analytical grade for buffer components and HPLC grade for solvents) and purchased from Sigma Aldrich Co. Thin layer chromatography combined with iodine staining was used regularly to check the purity and integrity of all lipids used (at least >99% on HPTLC plates) at various times after solubilization; no breakdown was observed during the course of our experiments (after solubilization and storage at −20 °C). All glasswares were cleaned using either concentrated H_2SO_4 or a concentrated KOH (~1.92 M; 24 g H_2O, 25 g KOH, and 164 g C_2H_5OH) cleaning solution to avoid contamination of stocks, water and buffer. The Teflon trough and stirrer were cleaned thoroughly before each monolayer experiment by several washes of detergent, distilled water, and KOH cleaning solution. The Wilhelmy plate was rinsed with chloroform, distilled water and KOH cleaning solution.

1.2. π-A isotherms

Langmuir monolayers were formed on two different Langmuir troughs. At the Advanced Photon Source (APS) of Argonne National Laboratories, the monolayers were spread in a temperature controlled (20 ± 1 °C) home built Langmuir monolayer trough in a gas-tight aluminum container and surface tension was recorded using a filter-paper Wilhelmy plate. Compression of the monolayers was performed asymmetrically at 1.8 $Å^2$ per molecule per minute. Langmuir monolayers for isotherm measurements were formed on a temperature controlled (20 ± 1 °C) KSV (KSV, Finland) mini-trough system and surface tension was recorded using a platinum Wilhelmy plate. Symmetric compression of the monolayer was made at 2.0 $Å^2$.molecule^{-1}.min^{-1}. The subphase used for all experiments was pH 7.2 buffer; 10 mM Tris–HCl, 150 mM NaCl, 0.2 mM EDTA. Water used in the experiments was purified by a Milli-Q system, Millipore Corp., Bedford, MA (at the APS) or by a PurelabPlus UV system (US Filter), for isotherm measurements and in both cases had a resistivity of 18.2 MΩ-cm and passed the shake test. Briefly, in the shake test one tests small air bubbles that are formed during shaking of a water containing flask immediately break through the surface when they reach the air–water interface [26].

1.3. Insertion isotherms

Insertion isotherms were performed at room temperature according to [20], in a Plexiglas enclosure. The circular Teflon trough was filled with 6.5 mL of the Tris buffer used as the subphase in this experiment. Temperature of the subphase was monitored within the enclosure and kept at 21 ± 2 °C, except as noted. Monolayers were formed at the air/buffer interface by the drop wise addition of the lipids dissolved in chloroform or chloroform/methanol on to the surface of the buffer using a Hamilton microsyringe until the desired initial surface pressure was reached. The solvent was allowed to evaporate for about 10 min before the introduction of apoLp-III into the subphase via injection with a micropipette through a hole at the side of the trough. Continuous mixing of the sub phase was ensured by a magnetic bar. The change in surface pressure with time was monitored with a platinum Wilhelmy plate and a conventional PS4 Nima surface pressure sensor. All experiments were carried out on a vibration-isolated table. The concentration of apoLp-III used for our experiments corresponds to the minimal amount of protein required to reach the maximum surface pressure of the apoLp-III monolayer, namely 0.11 μM (see Fig. 1).

The increase of surface pressure after protein injection as a function of initial lipid monolayer pressure results in curves that yield both the maximum insertion pressure (MIP) value and the maximal increase in surface pressure ($\Delta\pi_{max}$). The uncertainty of these values is determined by calculating the 95% confidence interval for both $\Delta\pi_{max}$ and MIP. For $\Delta\pi_{max}$ the 95% confidence interval is found by multiplying the SE, given by the SigmaPlot 11 software used to generate a linear fit, by 1.96. The 95% confidence interval for MIP is found as described by Calvez et al. [27].

1.4. X-ray scattering

X-ray studies at the gas–water (buffer) interface were conducted on the Ames Laboratory's liquid surface diffractometer at the APS, beamline 6ID-B as described in reference [28]. To reduce x-ray damage to the monolayer resulting from free radical and ion formation, and to decrease background scattering from air, the thermostated trough was kept under a water-saturated helium atmosphere. The trough was

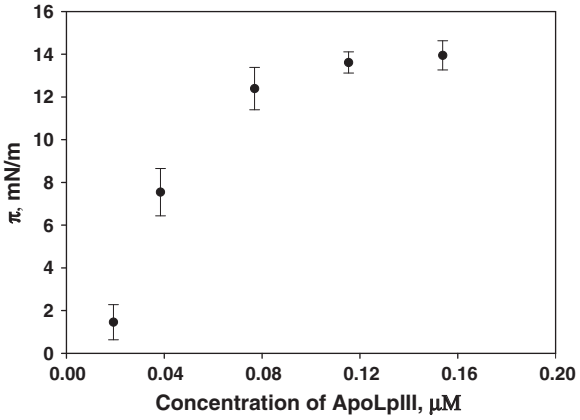

Fig. 1. Surface activity of apoLp-III. Injection of apoLp-III underneath a buffer-air interface leads to the self-assembly of an apoLp-III monolayer. Increased concentrations of apoLp-III in the subphase cause an increase in the surface pressure asserted by the self-assembled monolayer up to a maximum pressure. Subphase buffer: 10 mM Tris, 150 mM NaCl. 0.2 mM EDTA at pH 7.2.

mounted on a motorized stage that is easily translated laterally to inspect radiation damage by illuminating different parts of the monolayer. During the course of our experiments no significant radiation damage was observed as indicated by the reproducibility of reflectivity curves. The highly monochromatic beam (16.2 keV, $\lambda = 0.765334$ Å) was selected by a downstream Si double crystal monochromator and was deflected onto the liquid surface to a desired angle of incidence with respect to the liquid surface by a second monochromator (Ge(220) crystal) located on the diffractometer.

X-ray reflectivity (XR) in combination with grazing incidence x-ray diffraction (GIXD) is a common technique to investigate the detailed molecular arrangements in monomolecular layers at the air-liquid interface [28,29]. Specular XR experiments yield the electron density (ED) profiles across the interface and can be related to the molecular structure of the film. The electron density profile across the interface is obtained by a two-stage refinement of a slab model that best fits the measured reflectivity by the nonlinear least-squares method. The ED profile $\rho(z)$ is constructed by a sum of error functions:

$$\rho(z) = \frac{1}{2}\sum_{i=1}^{N+1} \mathrm{erf}\left(\frac{z-z_i}{\sqrt{2}\sigma}\right)(\rho_i - \rho_{i+1}) + \frac{\rho_1}{2} \quad (1)$$

where $N + 1$ is the number of interfaces; σ is the surface roughness $(\rho_i - \rho_{i+1})$; z_i are the change in the ED and the position of the i^{th} interface, respectively; ρ_1 is the ED of the subphase ($\approx$0.336 e/Å^3 for buffer subphase); and $\rho_{N+2} \approx 0$ is the density of the gas phase. The variable parameters are ρ_i, z_i (the thickness of the slabs associated with different parts of the molecules are denoted as $d_i \equiv |z_i - z_{i-1}|$), and the roughness σ_i. The continuous ED is sliced into a histogram (several hundred slices) to compute the reflectivity using the recursive dynamical method [28,30–32]. Errors for the fit parameters were determined by finding the variation in each of the parameters that resulted in a 50% increase in the χ^2 (measure of the goodness of the fit) of the fit with readjusting all other parameters.

GIXD experiments were conducted to determine the lateral organization in the film. In these experiments, the angle of the incident beam with respect to the surface, α, is fixed below the critical angle ($\alpha_c = \lambda(\rho_s r_0/\pi)^{1/2} = 0.0759$ deg., where λ is the x-ray wavelength (depends on x-ray energy used, here 16.2 keV), $r_0 = 2.82 \times 10^{-13}$ cm is the classical electron radius (where ρ_s is the subphase ED) for total reflection, while the diffracted beam is detected at a finite azimutal in-plane angle, 2Θ, and out-of-plane angle, β (the angle of the reflected beam with respect to the surface). Rod-scans (the intensity distribution of the 2D Bragg reflections normal to the surface) determine the average ordered chain length and tilt angle with respect to the surface normal. This intensity distribution is usually analyzed in the framework of the distorted wave Born approximation [28,33].

The coordinate system is chosen such that Q_z is normal to the liquid surface, Q_x is parallel to the horizontal (untilted) incident x-ray beam, and Q_y is orthogonal to both Q_z and Q_x. The hydrocarbon chains of saturated diacylglycerol form two-dimensional poly-crystals, giving rise to a diffraction pattern that depends on the modulus of the in-plane momentum transfer $Q_{xy} = \sqrt{\left(Q_x^2 + Q_y^2\right)}$, and is practically independent of rotation of the sample over the z-axis. The GIXD data are plotted as intensity vs. Q_{xy}.

2. Results and discussion

Here we use apoLp-III from *L. migratoria* as model exchangeable protein to investigate in detail the specificity of the interaction with (phospho-) lipids using Langmuir monolayer techniques and the organization of the protein at the interface using surface sensitive x-ray reflectivity and diffraction.

2.1. Structure of apoLp-III at the air–buffer interface

As model system we utilize lipid, protein, and protein–lipid monolayers at the air–buffer interface. In order to determine the optimum amount of protein for protein insertion isotherms and to investigate to what degree apoLp-III is surface active by itself we investigated the self-assembly of apoLp-III after injection into a buffer (10 mM Tris, 150 mM NaCl, pH 7.2) as a function of apoLp-III subphase concentration. Fig. 1 clearly shows that increased concentrations of apoLp-III lead to increased surface pressure of the self-assembled monolayer up to a plateau (saturation) pressure of ~14 mN/m. From these results we determined the optimum concentration of apoLp-III for our insertion experiments to be 0.11 μM. We assume here that for each of the lipid monolayers investigated this also saturates the protein–lipid interaction. This is verified by the observation that additional injection of apoLp-III underneath the lipid monolayer does not result in a further increase in surface pressure. In our typical insertion experiments this translates into 12.5 μg of protein (for a subphase volume of 6.5 ml, and a MW of apoLp-III of 20 kD).

Proteins can aggregate and denature at surfaces, so it is important to verify whether or not this is the case for apoLp-III [27]. Soluble apoLp-III forms an amphipathic α-helix bundle (which forms a cylinder with diameter 22 Å and length 53 Å [34]). In the lipid bound form these helices unfold, i.e. undergo a large conformational change, with the hydrophilic face positioned to interact with water and the hydrophobic face with lipid. To study the structure of potentially unfolded apoLp-III at the air–buffer interface, we performed x-ray reflectivity which determines the electron density across the interface. Results for self-assembled apoLp-III monolayers at the interface and for those deposited by careful placement of small drops of a 1 mg/ml apoLp-III solution at the interface and compression of the subsequent layer were found to behave very similar (data not shown). Fig. 2 shows x-ray reflectivity results for a monolayer of native apoLp-III at the air–buffer interface at 18 mN/m and the resultant electron density calculated from these data. Clearly the reflectivity is distinct from a "clean" air–buffer interface as indicated by the dashed line in Fig. 2A which represents the calculated reflectivity from a flat buffer (calculated ED 0.336 electrons/Å^3) interface. The best fit to the data shows two distinct regions of ED and not just one as might be expected for an unfolded amphipathic α-helix bundle protein (see Fig. 2B). The main contribution to the interface electron density is formed by the individual amphipathic α-helices of the helix-bundle unfolded at the interface. The thickness of this region, ~11 Å, corresponds well with the anticipated width of a protein α-helix (see e.g. [35]).

Below this layer formed by the amphipathic helices of apoLp-III, lies a diffuse region of ED. This region could originate from either the

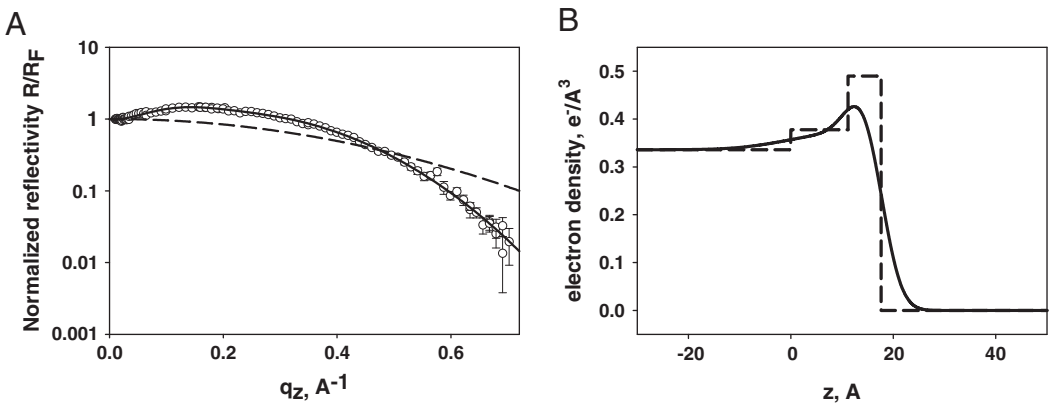

Fig. 2. XRR data for a self-assembled monolayer of native apoLp-III. (A) Reflectivity from native apoLp-III at 18 mN/m on a 10 mM Tris, 150 mM NaCl, 0.2 mM EDTA, pH 7.2 subphase. Solid black line is the best fit to the data and the blue line is calculated for a bare buffer/vapor surface including surface roughness due to capillary waves. (B) The calculated electron density from the best fit to the data shown in A. The step wise electron density shows the distinct "boxes" without roughness between them.

glycosylation of native apoLp-III (the ED in this region correlates with that of dilute carbohydrate solutions) or the flexible loops that connect the amphipathic α-helices of the helix bundle. In order to distinguish between these two scenarios we repeated the x-ray reflectivity experiment with a recombinant form of the protein that lacked the carbohydrate groups. The x-ray reflectivity of recombinant apoLp-III was identical to that of the native protein (see supplementary Fig. S1A). These data thus suggest the α-helix bundle of apoLp-III unfolds at hydrophobic interfaces with the flexible loops that connect the 5 amphipathic α-helices exposed in the solution, away from the interface. Additionally grazing incidence x-ray diffraction of native and recombinant apoLp-III at sufficiently high surface pressure (<15 mN/m) exhibits a very weak and broad peak that corresponds to a d-spacing of ~10 Å indicating short range organizational order between the individual amphipathic α-helices (see supplementary Fig. S1A). This peak is more pronounced for the recombinant protein, suggesting the native protein carbohydrate chains hinder the interaction between neighboring amphipathic α-helices.

2.2. Insertion of apoLp-III into a diacylglycerol monolayer

Most insect lipophorin transports not triacylglycerols but diacylglycerols, and apoLp-III interacts strongly with diacylglycerol exposed at the phospholipid–protein monolayer covering the lipophorin particle. Soulages and coworkers showed that concentrations as low as 2 mol % trigger apoLp-III–lipid binding [21]. What is not clear is whether or not this lipid binding is chemically specific or simply a function of the differential packing (i.e. physical) properties of diacylglycerol. More generally the question can be stated as follows: "What is the driving force behind lipid binding of amphipathic α-helix bundle proteins such as apoLp-III?" The generally accepted model is that hydrophobic defects on the surface of the lipoprotein particle trigger protein binding [8,21]. However this does not satisfactorily answer the question as it does not address the specific type of hydrophobic defect. Three distinct modes of hydrophobic interaction can be considered that might drive the interaction, namely,

i. Hydrophobic interactions arising from packing defects between the lipids making up the monolayer covering the droplet, which thus depend on packing density.
ii. Hydrophobic "defects" arising from a mismatch in effective molecular area between lipid headgroup and acyl-chain area, i.e. the spontaneous curvature of the lipid making up the lipid monolayer. Increases in negative curvature stress in the monolayer, leaving more room in the headgroup region, would facilitate apolar protein contacts, whereas additional positive curvature stress would impede monolayer insertion. Note that these defects, unlike the ones in (i), are delocalized over the entire monolayer. The definition of negative and positive lipid (monolayer) curvature was defined by Helfrich in his seminal work from 1973 and is now common convention [36].
iii. Hydrophobic "defects" arising from line boundaries between different lipid and lipid/protein domains on the surface of the particle [37].

The first two of these hydrophobic interactions are addressed by our Langmuir monolayer insertion studies that utilize lipids that fall within the range of lipids found in insect lipophorin. Our choice of (phospho-) lipids also systematically addresses these apolar interactions. The third hydrophobic interaction, domain boundaries, will be touched upon in the discussion. The first (i) hydrophobic defect is addressed by measuring the insertion, a requirement for stable incorporation into the surface monolayer, as a function of lipid molecular area (as expressed by the surface pressure). The second (ii) is addressed by choosing lipids that differ in their spontaneous curvature.

Diacylglycerol, due to its high negative spontaneous curvature (i.e., it is cone-shaped, see Fig. 9)), creates so-called hydrophobic defects in a phospholipid monolayer as shown recently by Vamparys et al. [38] and further investigated by Vanni et al. [39] in an accompanying paper. Vamparys compared the packing defects created by diacylglycerol to those created by high positive curvature of a lipid bilayer leaflet and concluded that both types act in the same way to recruit hydrophobic domains/residues to the membrane.

2.2.1. Characterization of diacylglycerols used

We thus characterized the lipid packing properties of three diacylglycerols, namely dipalmitoyl-glycerol (1,2-DPG), dioleoylglycerol (1,2-DOG) and 1-palmitoyl-2-oleoyl-sn-glycerol(1,2-POG) as Langmuir monolayers at the air–buffer interface. Representative isotherms at 20 °C are shown in Fig. S2. Next we investigated the packing properties via x-ray reflectivity and diffraction techniques sensitive to a monomolecular layer at the air–buffer interface. Both 1,2-DOG and 1,2-POG formed well-defined layers as shown by the reflectivity data in Fig. 3A and C respectively. The electron density calculated from these reflectivity profiles is shown in Fig. 3B and D, respectively, parameters shown in Table 1A and 1B. Both 1,2-DOG and 1,2-POG show differential packing behavior as a function of monolayer pressure (i.e. molecular area). At low pressure (10 mN/m and below) the 1,2-DOG and 1,2-POG monolayer electron density changes more gradually between the acyl chain and headgroup region because of the larger area per lipid. The structure changes to a higher and more tightly packed headgroup region at 25 mN/m and above. It should be noted that the ED of both of these diacylglycerols are highly similar, in agreement with their corresponding isotherm (Fig. S2). In 1,2-POG an additional transition is present at

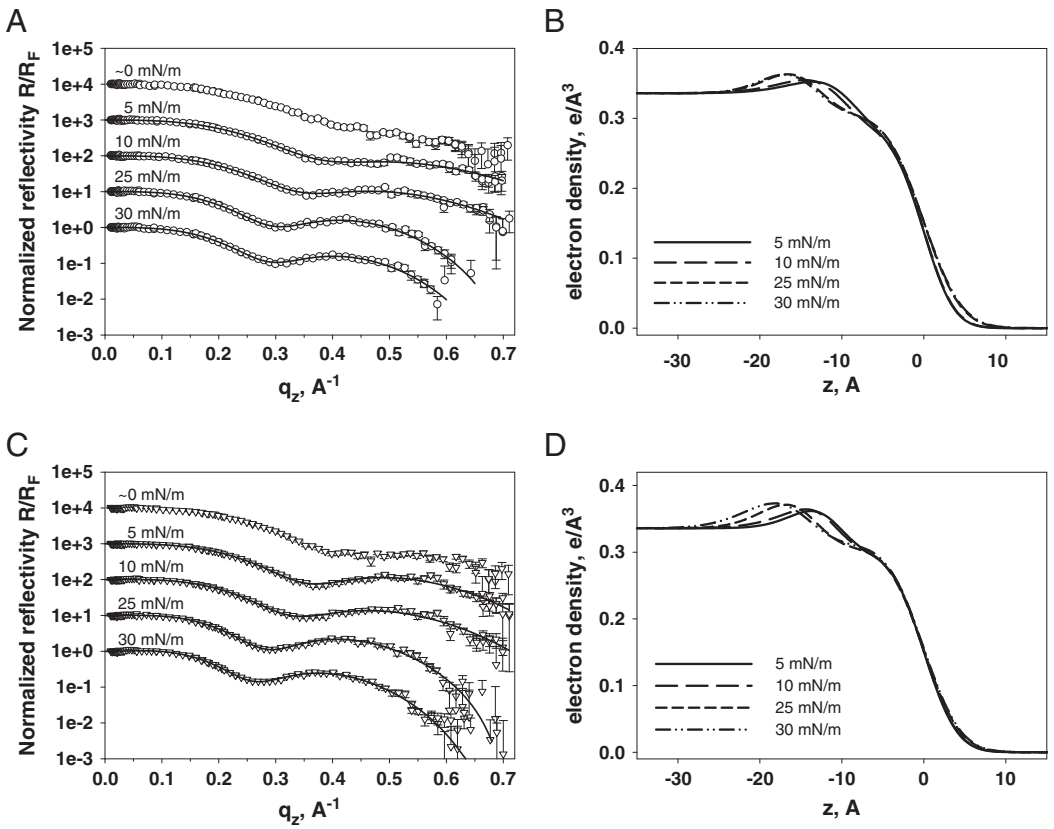

Fig. 3. XRR data for two diacylglycerols as a function of surface pressure. (A) X-ray reflectivity data for dioleoylglycerol (1,2-DOG) as a function of surface pressure(shifted by a decade each for clarity). (B) Electron density profiles for 1,2-DOG as a function of surface pressure. (C) X-ray reflectivity data for 1-palmitoyl-2-oleoyl-glycerol (1,2-POG) as a function of surface pressure. (D) Electron density profiles for POG as a function of surface pressure. The ED are calculated from the best fit to the reflectivity data. Fitting parameters are shown in Table 1A and 1B.

30 mN/m that coincides with the appearance of a diffuse peak in the x-ray diffraction.

X-ray diffraction for 1,2-DOG did not result in any discernible diffraction from the acyl chains. This was not unexpected given the unsaturation of the oleoyl acyl chains that are known to be disordered. By contrast, we did observe a weak diffraction signal from the 1,2-POG monolayer at high (>25 mN/m) surface pressure despite the presence of one unsaturated (double bond at: Δ^{9cis}) chain in this lipid (shown in Fig. S3). This diffraction corresponds to an additional packing transition observed in the reflectivity data (see Fig. 3D), which is markedly less than that observed in, for example, long chain saturated fatty acids or saturated phospholipids as indicated by the diffraction from a cer-1-p monolayer plotted in gray for comparison (in Fig. S3) [40]. The low intensity of the diffraction suggests the correlation length is finite (i.e. only short range order). The palmitoyl chain must assist in ordering the oleoyl chain at high pressure. We did not further investigate the 1,2-DPG monolayer due to the finding that DPG forms a solid monolayer at the air–buffer interface (see isotherm in Fig. S2). Additionally, the insertion experiments with DPG did not yield consistent results (data not shown). Since 1,2-DPG forms a solid monolayer at any appreciable surface pressure (see Fig. S2) it was experimentally difficult to form monolayers of defined initial surface pressure by sequentially applying small volumes of lipid stock solution to reach the desired initial lipid pressure, the method used by us and others (see, e.g. [20]) to make lipid monolayers for the insertion experiments.

The effect of apoLp-III insertion into monolayers of 1,2-DOG and 1,2-POG is shown in Fig. 4. The insertion of apoLp-III at low lipid monolayer pressure (large molecular area as seen from the isotherms in Fig. S2) leads to a large increase in the initial lipid monolayer pressure. This increase (at low lipid surface pressure) is larger for 1,2-POG than for 1,2-DOG as shown by the maximum insertion pressure, $\Delta\pi_{max}$, which is the increase in surface pressure upon protein insertion extrapolated to zero initial lipid monolayer pressure. The $\Delta\pi_{max}$ for 1,2-POG is 3 mN/m (95% confidence intervals do not overlap) higher than for 1,2-DOG. The increase is not due to a displacement of 1,2-DOG or 1,2-POG as the observed pressure is significantly higher than that of the self-assembled apoLp-III monolayer (Fig. 1, ~14 mN/m). Instead the increase in surface pressure is due to interaction of apoLp-III with 1,2-DOG and 1,2-POG. At increasingly higher lipid monolayer pressures the increase in surface pressure due to protein insertion decreases. Extrapolating this increase in lipid monolayer pressure upon protein insertion to zero leads to a lipid monolayer pressure called the maximum insertion pressure (MIP) [27], the lipid monolayer surface pressure above which

Table 1A
Fitting parameters for x-ray reflectivity data for 1,2-DOG shown in Fig. 3.

DOG data	5 (mN/m)	10 (mN/m)	25 (mN/m)	30 (mN/m)
σ_0 (Å)	3.14 ± 0.23	$3.12^{+0.20}_{-0.17}$	$3.48^{+0.15}_{-0.18}$	$3.57^{+0.18}_{-0.20}$
d_{head} (Å)	3.5 ± 1.5	$4.0^{+2.0}_{-1.0}$	$2.6^{+2.4}_{-0.6}$	$2.7^{+2.3}_{-0.7}$
ρ_{head} (e/Å^3)	$0.40^{+0.07}_{-0.03}$	$0.40^{+0.09}_{-0.02}$	$0.46^{+0.05}_{-0.07}$	$0.46^{+0.06}_{-0.07}$
d_{chain} (Å)	$10.3^{+1.4}_{-1.0}$	$11.1^{+1.5}_{-0.6}$	$14.3^{+0.7}_{-1.6}$	$14.6^{+0.9}_{-1.6}$
ρ_{chain} (e/Å^3)	$0.292^{+0.015}_{-0.012}$	$0.288^{+0.022}_{-0.011}$	$0.299^{+0.007}_{-0.009}$	$0.299^{+0.007}_{-0.010}$

Table 1B
Fitting parameters for x-ray reflectivity data for 1,2-POG shown in Fig. 3.

	5 (mN/m)	10 (mN/m)	25 (mN/m)	30 (mN/m)
σ_0 (Å)	$3.11^{+0.15}_{-0.22}$	$3.15^{+0.19}_{-0.21}$	3.37 ± 0.16	$3.38^{+0.16}_{-0.17}$
d_{head} (Å)	$2.3^{+2.7}_{-0.3}$	$2.9^{+2.1}_{-0.9}$	3.5 ± 1.5	$3.1^{+1.9}_{-1.1}$
ρ_{head} (e/Å^3)	$0.47^{+0.04}_{-0.08}$	$0.45^{+0.07}_{-0.06}$	$0.44^{+0.10}_{-0.04}$	$0.46^{+0.09}_{-0.05}$
d_{chain} (Å)	$11.7^{+0.6}_{-1.5}$	$12.4^{+0.9}_{-1.3}$	14.5 ± 1.1	$14.7^{+1.0}_{-1.3}$
ρ_{chain} (e/Å^3)	$0.293^{+0.009}_{-0.014}$	$0.297^{+0.008}_{-0.013}$	$0.301^{+0.006}_{-0.008}$	$0.302^{+0.006}_{-0.008}$

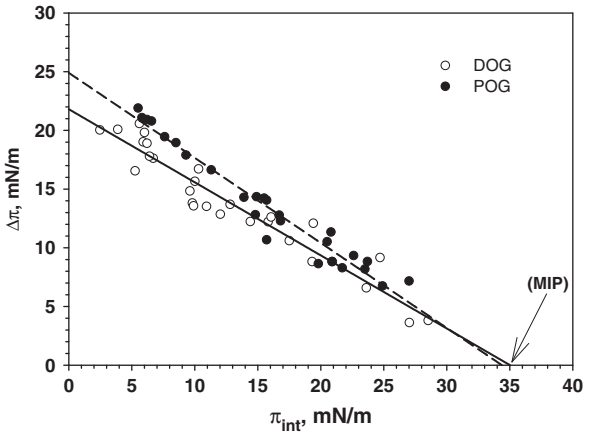

Fig. 4. Change in surface pressure versus initial lipid monolayer pressure after interaction with apoLp-III for1,2-DOG and 1,2-POG. Subphase buffer: 10 mM Tris, 150 mM NaCl, 0.2 mM EDTA at pH 7.2.

Table 2
The maximal increase in the surface pressure ($\Delta\pi_{max}$) and the maximum insertion pressure (MIP) after insertion of apoLp-III for the different lipids is shown. The 95% confidence interval (±value) is also shown and was calculated as described in Materials and methods.

	$\Delta\pi_{max}$ (mN/m)	MIP (mN/m)		$\Delta\pi_{max}$ (mN/m)	MIP (mN/m)
DOG	21.8 ± 1.2	35.0 ± 1.0	POG	24.9 ± 1.2	34.4 ± 0.7
DOPE	17.3 ± 1.6	28.6 ± 1.4	POPE	18.7 ± 1.4	30.1 ± 1.5
DOPC	17.3 ± 2.0	26.3 ± 1.0	POPC	18.1 ± 1.2	26.9 ± 1.0
DOPG	19.9 ± 1.8	26.4 ± 1.2	POPG	20.6 ± 1.2	29.2 ± 1.8

apoLp-III is no longer able to insert itself into the lipid layer. Further insertion of apoLp-III no longer results in a decrease of the surface free energy beyond this lipid monolayer pressure. For DOG we find a MIP, 35.0 ± 1.0 mN/m, identical to that found previously by Demel et al. [20]. The MIP for POG (MIP = 34.4 ± 0.7) is the same as that of DOG (see Table 2).

2.3. Insertion of native apoLp-III into phospholipid monolayers; effect of headgroup and acyl-chain species

Next, we systematically varied the headgroup and acyl-chain composition of the lipid monolayer to modulate both the spontaneous curvature and chemical nature of the lipids (see Table 3). We determined the $\Delta\pi_{max}$ and MIP of native apoLp-III for each of these lipids (see Table 2).

In order to study the effect of chemical species (chemical specificity and charge) and hydrophobic defects of type i and ii (localized packing defects vs. effective lipid molecular shape), we varied the lipid headgroup, charge, and acyl-chain composition. The lipid headgroups were (1) phosphocholine, (2) phosphoethanolamine and (3) phosphoglycerol. The acyl-chains chosen were 1,2-dioleoyl, and 1-palmiltoyl, 2-oleoyl. These lipids are summarized in Table 3 together with their relevant physical and chemical properties.

For diacylglycerol (1,2-DOG and 1,2-POG) we observed a MIP around 35 mN/m. Since diacylglycerol is a neutral lipid with strong negative spontaneous curvature [41,42], and to further investigate the effect of spontaneous curvature on apoLp-III insertion we used DOPE, a lipid with strong negative curvature, if not as strong as that of 1,2-DOG and 1,2-POG ($C_{DOPE} \cong -1/30$ Å^{-1} [41,43], whereas $C_{DOG} \cong -1/10.1$ Å^{-1} [41,42]). If spontaneous curvature were a strong determinant for insertion of apoLp-III then one would expect DOPE to show more insertion than DOPC, a lipid with very small ($-1/143$ to $-1/200$ Å^{-1}, i.e. essentially zero) spontaneous curvature [42]. Data shown in Fig. 5 and summarized in Table 2 suggests that while DOPE allows slightly more insertion of apoLp-III into the lipid monolayer, the increase in MIP of DOPE over that for DOPC is very minor (95% confidence intervals overlap). This increase is much less than that for 1,2-DOG and 1,2-POG.

Next, we investigated the effect of negative charge on the interaction of apoLp-III with a lipid monolayer. We chose DOPG because its spontaneous curvature has been characterized (identical to that of DOPC; $C_{DOPG} = -1/150$ Å^{-1} [44]). The use of PG is not only interesting because of its negatively charged headgroup but also due to the fact that PG is an important bacterial lipid. Investigating the interaction of apoLp-III with PG has implications for the immune response in insects. For example, apoLp-III from *Galleria mellonella* has been implicated in the immune response [45–47]. The immune protective function of apoLp-III is not unique as it has also been found for apoA-I, apoE, and apoB [48–51]. Interestingly we observe that the $\Delta\pi_{max}$ pressure for DOPG is larger (by 2.5 mN/m) than for DOPC and DOPE suggesting that the negative charge aids in the recruitment of apoLp-III to the lipid monolayer. This is consistent with the finding that apoLp-III of *L. migratoria* contains several basic amino acid residues on the hydrophilic face of the amphipathic α-helix bundle, similar to what is found on apoA-I [48]. On the other hand, the MIP of apoLp-III for a DOPG monolayer is identical to that for DOPC, consistent with their spontaneous curvature.

Next we changed the acyl-chain composition to investigate the effect of chain saturation while maintaining an essentially fluid lipid monolayer (i.e. at 20 °C these lipids form a liquid disordered monolayer at low pressures and a liquid ordered monolayer at high pressure). The MIP curves for the 1-palmitoyl, 2-oleoyl containing phospholipids are shown in Fig. 5B. Compared with the data for the dioleoyl lipids we find that the MIP for POPE, POPG and POPC are very similar and significantly different from that of 1,2-POG. Interestingly we find that the MIP follows a slightly different trend namely that the MIP for POPC is the smallest followed by those of POPE and POPG (which are essentially identical) with the highest value observed for 1,2-POG. This is opposite from the trends in the dioleoyl data where we found that the MIP for DOPC and DOPG were identical. This observation is further discussed below.

Table 3
List of glycero-(phospho)-lipids used in this study.

Lipid	Abbreviation	Charge	Chains	"Curvature"‡
1-2-Dioleoyl-*sn*-glycerol	DOG	Neutral	Unsaturated	Induces H_{II} phase
1-Palmitoyl-2-oleoyl-*sn*-glycerol	POG	Neutral	Mixed	Induces H_{II} phase
1,2-Dioleoyl-*sn*-glycero-3-phosphocholine	DOPC	Zwitterionic	Unsaturated	Bilayer
1-Palmitoyl-2-oleoyl-*sn*-glycero-3-phosphocholine	POPC	Zwitterionic	Mixed	Bilayer
1,2-Dioleoyl-*sn*-glycero-3-phosphoethanolomine	DOPE	Zwitterionic	Unsaturated	H_{II} phase
1-Palmitoyl-2-oleoyl-*sn*-glycero-3-phosphoethanolamine	POPE	Zwitterionic	Mixed	H_{II} phase
1,2-Dioleoyl-*sn*-glycero-3-phospho-(1′-*rac*-glycerol)*	DOPG	Anionic	Unsaturated	Bilayer
1-Palmitoyl-2-oleoyl-*sn*-glycero-3-phospho-(1′-*rac*-glycerol)	POPG	Anionic	Mixed	Bilayer

* Phosphatidylglycerol is used here as model anionic lipid and because it is an important bacterial phospholipid relevant to the immune protective function of apoLp-III [45–47].
‡ Information on the spontaneous curvature can be found in the review by Zimmerberg and Kozlov [63]. Additionally, an excellent resource for phase behavior information can be found in [64] (see for example pp. 539 and 767).

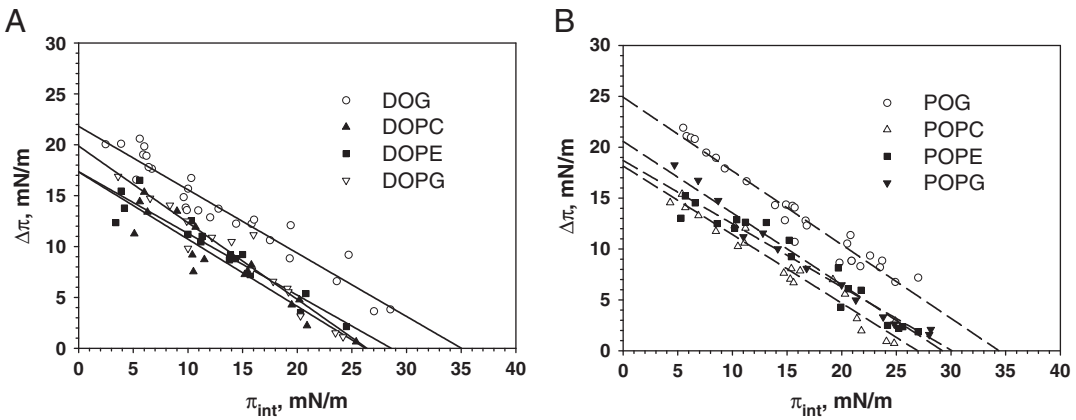

Fig. 5. Change in surface pressure versus initial lipid monolayer pressure after interaction with apoLp-III. (A) Insertion of apoLp-III into monolayers of 1,2-DOG, DOPC, DOPE, and DOPG. (B) Insertion of apoLp-III into monolayers of 1,2-POG, POPC, POPE, and POPG. Subphase buffer: 10 mM Tris, 150 mM NaCl, 0.2 mM EDTA at pH 7.2.

2.4. Effect of chain saturation and increased acyl-chain order

The insertion of native apoLp-III into monolayers containing saturated acyl-chains is more favorable than those containing two unsaturated chains. This is particularly striking for the 1,2-POG and 1,2-DOG monolayers as shown in Fig. 4, but also clear from the data for DOPG and POPG shown together in Fig. 6A. In fact, if we compare the best linear fit to our insertion data for all lipid headgroup species independently, the data for the more saturated lipid monolayer lie above that of the di-unsaturated lipid monolayer (See Fig. 6B and C). The data thus suggests that apoLp-III prefers a more ordered lipid monolayer for insertion. This observation was further tested by increasing the temperature of the POPG monolayer from 21 ± 2 °C to 26 ± 1 °C. Fig. 7 indeed shows that an increased temperature, and hence a decreased order in the POPG monolayer, leads to a decreased insertion of apoLp-III into the lipid monolayer.

2.5. Mixed native apoLp-III-diacylglycerol monolayers: refolding of apoLp-III?

Insertion of native apoLp-III into diacylglycerol monolayers was followed via x-ray reflectivity to determine the electron density across the lipid–protein–buffer interface. In these experiments we either injected apoLp-III underneath a preformed diacylglycerol monolayer at high surface pressure (>20 mN/m) or preformed a self-assembled protein monolayer and spread lipid from organic solution on top [52]. These layers were then either expanded or compressed or compressed and expanded. Several compression–decompression (or expansion–compression) cycles were followed by x-ray reflectivity while keeping x-ray damage to a minimum via a translational stage to minimize x-ray flux for any particular area.

Fig. 8 shows the reflectivity curves and corresponding ED from the best fit to the data for apoLp-III insertion into a 1,2-POG monolayer at ~29 mN/m (insertion at 20 mN/m yielded comparable results, data not shown). After insertion this layer was expanded to a molecular area corresponding to ~100 A^2 per 1,2-POG molecule. At this point the reflectivity clearly changed to correspond more to a protein only layer (compare reflectivity and ED to those of Fig. 2). This layer was subsequently compressed to the original area prior to expansion. The ED now corresponds with a POG monolayer with higher headgroup intensity due to further incorporation of apoLp-III into the lipid monolayer. These results are characteristic of similar experiments with 1,2-DOG and 1,2-DPG.

After insertion of apoLp-III in a diacylglycerol monolayer (1,2-DOG, 1,2-POG, or 1,2-DPG) at high (>20 mN/m) lipid monolayer pressure, the electron density of the lipid layer does not change significantly despite a significant increase in surface pressure (see Fig. 4). Expansion of the monolayer to larger areas per lipid leads to a shift of the electron density to that of the protein monolayer, and subsequent compression clearly shows a higher electron density for the headgroup region of the lipid monolayer (see Fig. 8). Previous observations showed that deposition of lipid on top of a preformed self-assembled protein monolayer leads to a similar increase in the surface pressure compared to insertion of protein underneath a lipid monolayer (at identical lipid densities) [52]. Our x-ray reflectivity data points out that this does not lead to a similar electron density profile. Deposition of DAG on top of a preformed apoLp-III monolayer results in a higher degree of protein incorporation directly after deposition (data not shown). However, a similar trend in electron density is observed upon compression–decompression cycles following this approach.

The results indicate that though more apoLp-III is incorporated in the lipid monolayer after expansion and compression, or right after deposition of lipid on top of a protein monolayer, the density of apoLp-III at the interface of a tightly packed lipid layer is insufficient to observe the protein. The protein α-helix is thus entirely embedded in the headgroup region (consistent with previous observations/suggestions, see e.g. [53]). Excess apoLp-III that moved from the subphase to the lipid–protein monolayer at high lipid molecular area is most likely expelled again after compression; however, folded apoLp-III is never observed underneath the lipid layer (within the time frame of the reflectivity experiment). This suggests that once apoLp-III is folded it diffuses away into the subphase. Several compression–decompression (or expansion–compression) cycles lead to significant hysteresis suggesting a loss of diacylglycerol from the interface, similar to that observed for the C-terminus of apo-A1 [54].

3. Conclusions

Interaction of native apoLp-III with lipid monolayers is more favorable for saturated acyl-chain containing lipids. This observation is consistent with a recent paper by Storey et al. that showed the lipid monolayer of perilipin enriched lipid droplets is more saturated than the biomembranes in the cell [55]. Both apoLp-III and TIP47/perilipin 3 have an amphipathic α-helix bundle, and our results for apoLp-III suggest that this forms a lipid sensor for more ordered lipid domains. Unfortunately there is limited data on the acyl-chain composition of the phospholipid monolayer covering low density lipophorin (LDLp) while more extensive data is available on the fatty acid composition of the core of these particles. The core of LDLp isolated from *L. migratoria* is enriched in C16:0 and C18:1 lipids, whereas that of the phospholipid monolayer is enriched in C18:0 and C18:2 and C18:3 fatty acids [18,19].

We did perform limited insertion experiments with 1,2-DPG and found insertion is not very reproducible and occurs even at high initial lipid monolayer pressures. A similar observation was made for POPE monolayers (data not shown). At high surface pressures POPE undergoes a phase transition to a more ordered phase. In this regime

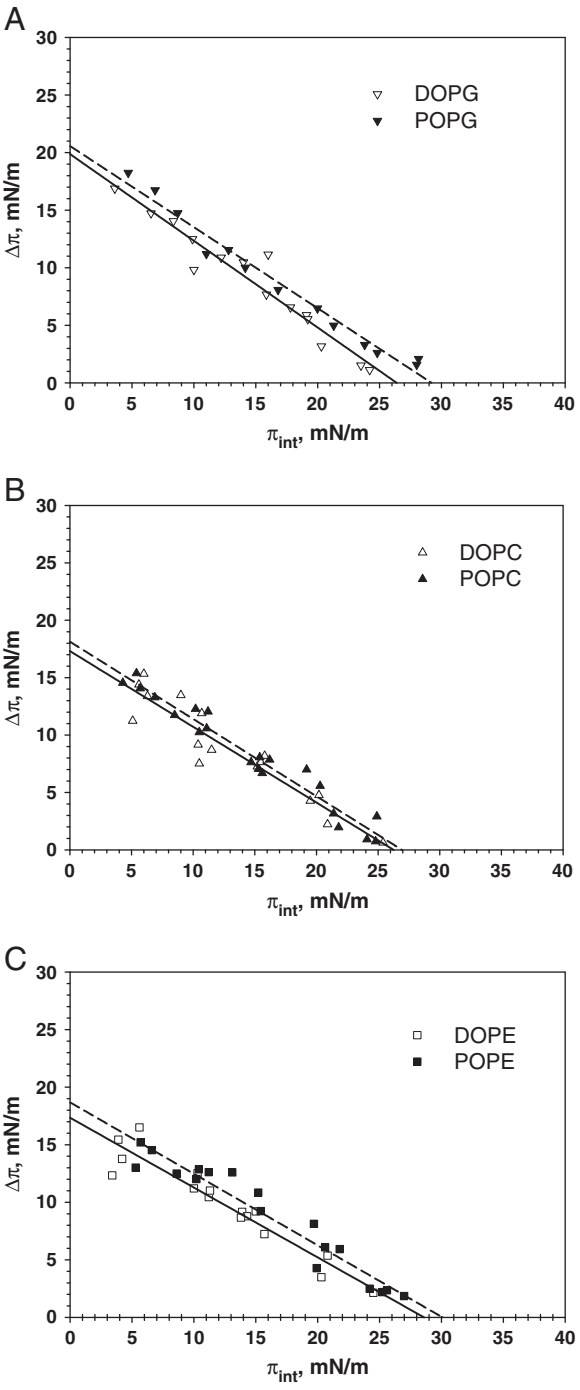

Fig. 6. Comparison of the insertion of apoLp-III into a di-unsaturated lipid monolayer and a phospholipid monolayer containing a *sn* 1-saturated, and 2-unsaturated lipid. (A) Insertion of apoLp-III into DOPG and POPG. (B) Insertion of apoLp-III into DOPC and POPC. (C) Insertion of apoLp-III into DOPE and POPE. Subphase buffer: 10 mM Tris, 150 mM NaCl, 0.2 mM EDTA at pH 7.2.

(π<35 mN/m) we routinely observe a limited amount of insertion in the range of 1–2 mN/m apparently independent of monolayer pressure. This observation is again consistent with the observation that apoLp-III interacts more favorably with saturated/ordered acyl chains.

An alternative explanation may be that apoLp-III interacts with line boundaries in the POPE and 1,2-DPG monolayer. Solid monolayers (as in 1,2-DPG) are only quasi 2-D crystals, as there is no real long-range order in individual molecule packing. Instead, these layers are built of many crystalline domains separated by domain boundaries. The structure of POPE monolayers at high pressure has been investigated

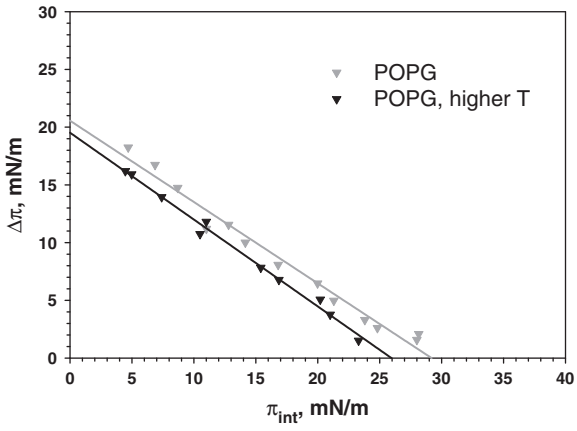

Fig. 7. Effect of increased temperature (increased fluidity) on the insertion of apoLp-III. Insertion of apoLp-III into a monolayer of POPG at 21 ± 2 °C with insertion of apoLp-III into a monolayer of POPG at 26 ± 1 °C. Subphase buffer: 10 mM Tris, 150 mM NaCl, 0.2 mM EDTA at pH 7.2.

via BAM microscopy and AFM spectroscopy [56–58]. In BAM, at low POPE surface pressures, tiny, brightly scattering specks are observed indicating some type of three dimensional structures ([56], and our own observations). The exact nature of these spots has not been studied to date. At the phase transition, clear domains become visible in both BAM and AFM with some of the bright spots still present. Domain formation at the phase transition appears to be reproducible. It is possible that apoLp-III–POPE interaction at high pressures is driven by this domain formation if apoLp-III has a high affinity for either one of the

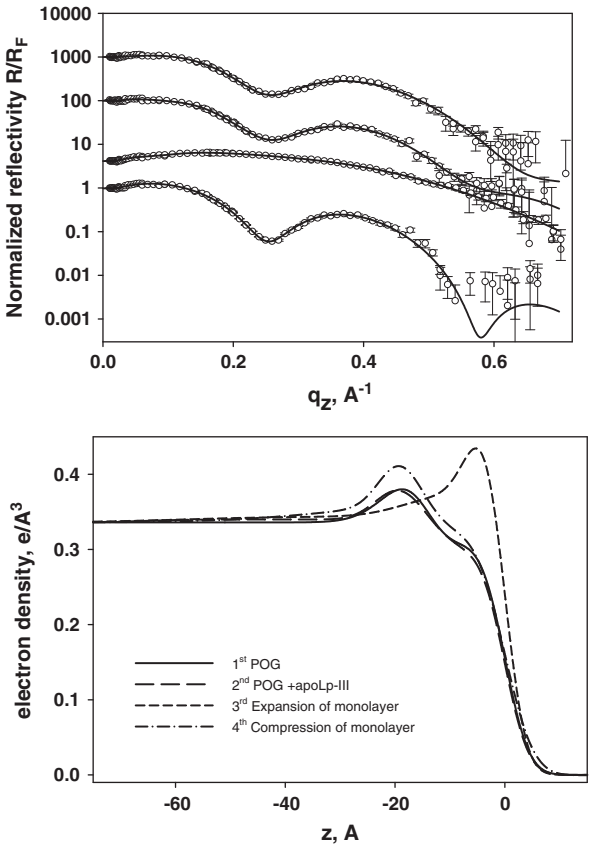

Fig. 8. Interaction of apoLp-III and 1,2-POG followed by XR. (A) Reflectivity curves from a monolayer of 1,2-POG at ~29 mN/m before and after interaction with apoLp-III and subsequent expansion and compression of the lipid–protein monolayer after compression and expansion. (B) Electron density profiles obtained from the best fit to the XR curves.

domains or for the domain boundaries. In the case of apoLp-III–1,2-DPG interaction it is possible that apoLp-III interacts with the boundaries surrounding each semi-crystalline domain. The finding by Wan et al. that apoLp-III is able to transform vesicles made of DMPC, or of shorter saturated lipids, into lipid nanodiscs [59], may be related to our observations. In the gel phase the DMPC vesicles consist of many connected gel phase domains and apoLp-III might be able to interact with these domain boundaries. However, apoLp-III is able to transform the lipid bilayer into lipid (membrane) nanodiscs only very near the phase transition. At the phase transition the compressibility of the bilayer is increased and hence deformability is likely enhanced. In light of the results from the disc assay it is timely to investigate the interaction of apoLp-III with domain boundaries in lipid monolayers. One possible method by which to explore this further is light scattering microscopy [60,61].

It is intriguing that the monolayers of perilipin-enriched lipid droplets contain more saturated phospholipid [55].Our results now show that a model amphipathic α-helix bundle protein interacts more favorably with more ordered lipid monolayers. This favorable interaction with more ordered lipid monolayers differentiates the lipid droplets monolayer from most other intracellular, and infinitely more abundant, lipid membranes. It is thus one mechanism by which TIP47/perilipin 3 may be sorted to growing lipid droplets surfaces.

This hypothesis is consistent with the finding that, e.g. caveolins, also reside on lipid droplets as their native membrane environment is more highly ordered than the rest of the plasma membrane. The high concentration of cholesterol in caveolae serves to order the lipid bilayer in these structures. So why then does, e.g. perilipin 3, not bind to caveolae? One reason might be that caveolae are formed by the simultaneous recruitment of caveolin and cholesterol and hence there is no additional space for perilipin 3; however, this suggestion clearly requires experimental verification.

The compression–decompression (or vice versa) experiments with diacylglycerol–apoLp-III monolayers show that apoLp-III is able to assemble from solution and unfold its helix bundle at the interface. Subsequent compression does not result in a folded helix-bundle attached to the lipid monolayer as far as our x-ray reflectivity experiments are able to observe. The results instead suggest that apoLp-III is able to quickly dissociate from the lipid monolayer as soon as the bundle has folded, consistent with its function in vivo.

3.1. Model of apoLp-III–preferential DAG interaction

Our results clearly show that insertion of apoLp-III into a monolayer of diacylglycerol is more favorable than into a monolayer of the six phospholipids that we tested here. One measure of this interaction is given by the $\Delta\pi_{max}$ and MIP data shown in Table 2. The maximum increase in the surface pressure gives an indication of the affinity of the protein to the lipid monolayer, whereas the MIP is an indication of the degree of insertion. For example, the higher $\Delta\pi_{max}$ for PG indicates some affinity of the protein for negative charge consistent with the basic amino acid residues; however, the degree of insertion is not increased as indicated by the MIP values.

We suggest that preferential interaction (as measured via the MIP) of apoLp-III with diacylglycerol is mediated by differences in headgroup size (steric interaction, length of the headgroup) of the lipid, and to a much smaller degree the spontaneous curvature (effective lipid molecular shape) of the lipids in the lipid monolayer. The cartoon in Fig. 9 shows this interaction model to scale.

Our data support this model in the following manner:

i) Insertion into a lipid monolayer is more favorable for DAG than PE and PC which both have a considerably larger headgroup. The depth at which the amphipathic α-helix has to insert in order to reach the hydrophobic interior of the lipid monolayer is considerably larger for PE and especially for PC than for DAG (see Fig. 9).

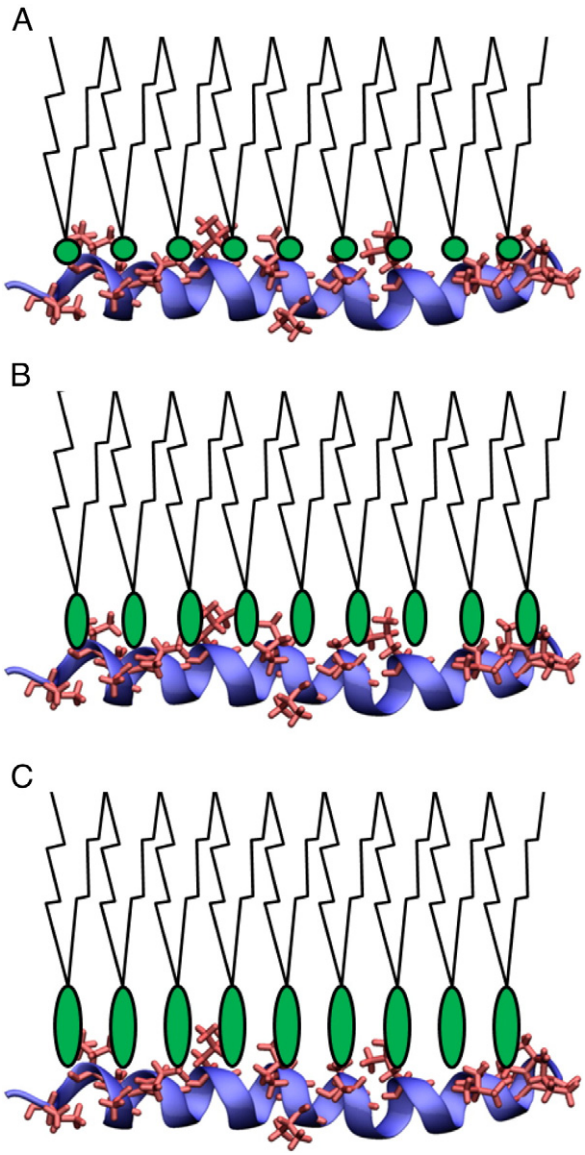

Fig. 9. Model of apoLp-III–lipid interaction. Schematic illustration of the first amphipathic α-helix of apoLp-III (residues 8–37, using pdb file 1LS4 [62]) interacting with (A) a diacylglycerol, (B) a phosphatidylethanolamine, and (C) a phosphatidylcholine monolayer. The α-helix is oriented such that the hydrophobic side is interacting with the lipid monolayer. The hydrophobic side residues are specifically depicted in the model. Lipid and protein are approximately to scale.

ii) Insertion into a monolayer containing saturated acyl-chain containing lipids was shown to be more favorable compared to unsaturated chains (with less order). This is especially evident when we compare 1,2-DOG and 1,2-POG at large molecular areas. At low initial lipid surface pressure the 1,2-DOG and 1,2-POG monolayer isotherms overlap (see Fig. S2). Insertion into a monolayer of these lipids in these conditions is considerably more favorable for 1,2-POG than for 1,2-DOG. 1,2-POG has a saturated acyl-chain at the sn-1 position and 1,2-DOG does not. Note that 1,2-POG is more ordered than 1,2-DOG,as also shown by the diffraction data (Fig. S3).

iii) The effect of a more ordered lipid monolayer was reiterated by the experiment where the POPG monolayer was heated. In this case we found a significantly reduced, over all molecular areas, insertion of apoLp-III into the POPG monolayer. Increased temperature means increased disorder for the acyl-chains of POPG. This thus follows the model where increased disorder in the

hydrophobic interior of the lipid monolayer significantly perturbs the interaction.

Interaction of hydrophobic side residues of apoLp-III with the hydrophobic interior of the lipid monolayer is thus crucial for apoLp-III–lipid interaction.

3.2. Future directions

These monolayer experiments on the model amphipathic α-helix bundle protein apoLp-III set the stage to investigate in exquisite detail the interaction of intracellular lipid droplets proteins containing this domain. Additionally, the interaction of human apolipoproteins such as apoE has not yet been examined in as much detail as we do here, i.e. different headgroups and acyl chain species that systematically vary lipid biophysical properties [27]. In addition to pure lipid monolayers, as in the present study, we will expand our work to include lipid mixtures with specific focus on the potential role of cholesterol. The interaction between LPS and apoLp-III of *G. mellonella* should be investigated as this will shed light on the immune protective function of apoLp-III.

Acknowledgments

Prof. Dick van der Horst and Dr. Kees Rodenburg are gratefully acknowledged for providing us with the native and recombinant apoLp-III from *L. migratoria*. Additionally we thank Prof. van der Horst for critically reading our manuscript and providing valuable suggestions. EEK gratefully acknowledges a Farris Family Fellowship award and Kent State University for support. An REU program in Chemistry (CHE-1004987) provided funds for undergraduate student researchers.

Use of the Advanced Photon Source (APS) was supported by the U.S. Department of Energy, Basic Energy Sciences, Office of Science (contract no. W-31-109-Eng-38). The Midwest Universities Collaborative Access Team sector at the APS is supported by the U.S. Department of Energy, Basic Energy Sciences, Office of Science. The work at Ames Laboratory was supported by the U.S. Department of Energy, Basic Energy Sciences, Office of Science (contract no. DE-AC02-07CH11358).

Any opinions, findings, and conclusions or recommendations expressed in this publication are those of the authors and do not necessarily reflect the views of the National Science Foundation.

Appendix A. Supplementary data

Supplementary data to this article can be found online at http://dx.doi.org/10.1016/j.bbamem.2013.09.020.

References

[1] V. Narayanaswami, R.O. Ryan, Molecular basis of exchangeable apolipoprotein function, Biochim. Biophys. Acta 1483 (2000) 15–36.
[2] P.M. Weers, R.O. Ryan, Apolipophorin III: a lipid-triggered molecular switch, Insect Biochem. Mol. Biol. 33 (2003) 1249–1260.
[3] P.M. Weers, R.O. Ryan, Apolipophorin III: role model apolipoprotein, Insect Biochem. Mol. Biol. 36 (2006) 231–240.
[4] R.O. Ryan, D.J. van der Horst, Lipid transport biochemistry and its role in energy production, Annu. Rev. Entomol. 45 (2000) 233–260.
[5] A.V. Bulankina, A. Deggerich, D. Wenzel, K. Mutenda, J.G. Wittmann, M.G. Rudolph, K.N. Burger, S. Honing, TIP47 functions in the biogenesis of lipid droplets, J. Cell Biol. 185 (2009) 641–655.
[6] S.J. Hickenbottom, A.R. Kimmel, C. Londos, J.H. Hurley, Structure of a lipid droplet protein; the PAT family member TIP47, Structure 12 (2004) 1199–1207.
[7] R.M. Hynson, C.M. Jeffries, J. Trewhella, S. Cocklin, Solution structure studies of monomeric human TIP47/perilipin-3 reveal a highly extended conformation, Proteins 80 (2012) 2046–2055.
[8] J.L. Soulages, M.A. Wells, Effect of diacylglycerol content on some physicochemical properties of the insect lipoprotein, lipophorin. Correlation with the binding of apolipophorin-III, Biochemistry 33 (1994) 2356–2362.
[9] M.A. Wells, R.O. Ryan, J.K. Kawooya, J.H. Law, The role of apolipophorin III in in vivo lipoprotein interconversions in adult *Manduca sexta*, J. Biol. Chem. 262 (1987) 4172–4176.
[10] J.K. Kawooya, S.C. Meredith, M.A. Wells, F.J. Kezdy, J.H. Law, Physical and surface properties of insect apolipophorin III, 2611986. 13588–13591.
[11] J.P. Shapiro, J.H. Law, Locust adipokinetic hormone stimulates lipid mobilization in *Manduca sexta*, Biochem. Biophys. Res. Commun. 115 (1983) 924–931.
[12] F.E. Thorngate, D.L. Williams, Lipoproteins, HDL/LDL, Encycl. Biol. Chem. 2 (2004) 588–593.
[13] J.P. Segrest, M.K. Jones, H. De Loof, C.G. Brouillette, Y.V. Venkatachalapathi, G.M. Anantharamaiah, The amphipathic helix in the exchangeable apolipoproteins: a review of secondary structure and function, J. Lipid Res. 33 (1992) 141–166.
[14] L.J. Vasquez, G.E. Abdullahi, C.P. Wan, P.M. Weers, Apolipophorin III lysine modification: effect on structure and lipid binding, Biochim. Biophys. Acta 1788 (2009) 1901–1906.
[15] K.D. Cole, M.A. Wells, A comparison of adult and larval *Manduca sexta* apolipophorin-III, Insect Biochem. 20 (1990) 373–380.
[16] M.P.J. De Winther, P.M.M. Weers, J. Bogerd, D.J. Van Der Horst, Apolipophorin III levels in *Locusta migratoria*. Developmental regulation of gene expression and hemolymph protein concentration, J. Insect Physiol. 42 (1996) 1047–1052.
[17] J.K. Kawooya, P.S. Keim, R.O. Ryan, J.P. Shapiro, P. Samaraweera, J.H. Law, Insect apolipophorin III. Purification and properties, J. Biol. Chem. 259 (1984) 10733–10737.
[18] A.M.T. Beenakkers, J.M.J.C. Scheres, Dietary lipids and lipid composition of the fat body of *Locusta migratoria*, Insect Biochem. I (1971) 125–129.
[19] Y. Peled, A. Tietz, Isolation and properties of a lipoprotein from the heamolymph of the locust, *Locusta migratoria*, Insect Biochem. 5 (1975) 61–72.
[20] R.A. Demel, J.M. van Doorn, D.J. Van Der Horst, Insect apolipophorin III: interaction of locust apolipophorin III with diacylglycerol, Biochim. Biophys. Acta 1124 (1992) 151–158.
[21] J.L. Soulages, Z. Salamon, M.A. Wells, G. Tollin, Low concentrations of diacylglycerol promote the binding of apolipophorin III to a phospholipid bilayer: a surface plasmon resonance spectroscopy study, Proc. Natl. Acad. Sci. U. S. A. 92 (1995) 5650–5654.
[22] A.M. Beenakkers, D.J. Van der Horst, W.J. Van Marrewijk, Insect lipids and lipoproteins, and their role in physiological processes, Prog. Lipid Res. 24 (1985) 19–67.
[23] J.E. Pennington, M.A. Wells, Triacylglycerol-rich lipophorins are found in the dipteran infraorder Culicomorpha, not just in mosquitoes, J. Insect Sci. 2 (2002) 15.
[24] D.J. Van der Horst, J.M. Van Doorn, H. Voshol, M.R. Kanost, R. Ziegler, A.M. Beenakkers, Different isoforms of an apoprotein (apolipophorin III) associate with lipoproteins in *Locusta migratoria*, Eur. J. Biochem. 196 (1991) 509–517.
[25] P.M. Weers, J. Wang, D.J. Van der Horst, C.M. Kay, B.D. Sykes, R.O. Ryan, Recombinant locust apolipophorin III: characterization and NMR spectroscopy, Biochim. Biophys. Acta 1393 (1998) 99–107.
[26] O. tradition.
[27] P. Calvez, S. Bussieres, D. Eric, C. Salesse, Parameters modulating the maximum insertion pressure of proteins and peptides in lipid monolayers, Biochimie 91 (2009) 718–733.
[28] D. Vaknin, in: E.N. Kaufmann (Ed.), Characterization of Materials, vol. 2, John Wiley & Sons, New York, 2012, pp. 1393–1423.
[29] J. Als-Nielsen, K. Kjaer, in: T. Riste, D. Sherrington (Eds.), Phase Transitions in Soft Condensed Matter, Plenum, New York, 1989.
[30] M. Born, E. Wolf, Principles of Optics, McMillan, New York, 1959.
[31] W. Bu, D. Vaknin, A. Travesset, How accurate is Poisson-Boltzmann theory for monovalent ions near highly charged interfaces? Langmuir 22 (2006) 5673–5681.
[32] L.G. Parrat, Phys. Rev. 59 (1954) 359.
[33] K. Kjaer, Some simple ideas on x-ray reflection and grazing-incidence diffraction from thin surfactant films, Physica B 198 (1994) 100.
[34] D.R. Breiter, M.R. Kanost, M.M. Benning, G. Wesenberg, J.H. Law, M.A. Wells, I. Rayment, H.M. Holden, Molecular structure of an apolipoprotein determined at 2.5-A resolution, Biochemistry 30 (1991) 603–608.
[35] D.L. Nelson, M.M. Cox, Lehninger, Principles of Biochemistry, 6th ed. W. H. Freeman and Company, 2012.
[36] W. Helfrich, Elastic properties of lipid bilayers: theory and possible experiments, Z. Naturforsch. C. 28 (1973) 693–703.
[37] T. Hevonoja, M.O. Pentikainen, M.T. Hyvonen, P.T. Kovanen, M. Ala-Korpela, Structure of low density lipoprotein (LDL) particles: basis for understanding molecular changes in modified LDL, Biochim. Biophys. Acta 1488 (2000) 189–210.
[38] L. Vamparys, R. Gautier, S. Vanni, W.F. Bennett, D.P. Tieleman, B. Antonny, C. Etchebest, P.F. Fuchs, Conical lipids in flat bilayers induce packing defects similar to that induced by positive curvature, Biophys. J. 104 (2013) 585–593.
[39] S. Vanni, L. Vamparys, R. Gautier, G. Drin, C. Etchebest, P.F. Fuchs, B. Antonny, Amphipathic lipid packing sensor motifs: probing bilayer defects with hydrophobic residues, Biophys. J. 104 (2013) 575–584.
[40] E.E. Kooijman, D. Vaknin, W. Bu, L. Joshi, S.W. Kang, A. Gericke, E.K. Mann, S. Kumar, Structure of ceramide-1-phosphate at the air–water solution interface in the absence and presence of Ca2 +, Biophys. J. 96 (2009) 2204–2215.
[41] S. Leikin, M.M. Kozlov, N.L. Fuller, R.P. Rand, Measured effects of diacylglycerol on structural and elastic properties of phospholipid membranes, Biophys. J. 71 (1996) 2623–2632.
[42] J.A. Szule, N.L. Fuller, R.P. Rand, The effects of acyl chain length and saturation of diacylglycerols and phosphatidylcholines on membrane monolayer curvature, Biophys. J. 83 (2002) 977–984.
[43] E.E. Kooijman, V. Chupin, N.L. Fuller, M.M. Kozlov, B. de Kruijff, K.N.J. Burger, P.R. Rand, Spontaneous curvature of phosphatidic acid and lysophosphatidic acid, Biochemistry 44 (2005) 2097–2102.
[44] S.H. Alley, O. Ces, M. Barahona, R.H. Templer, X-ray diffraction measurement of the monolayer spontaneous curvature of dioleoylphosphatidylglycerol, Chem. Phys. Lipids 154 (2008) 64–67.
[45] G. Dunphy, A. Halwani, Haemolymph proteins of larvae of Galleria mellonella detoxify endotoxins of the insect pathogenic bacteria Xenorhabdus nematophilus (Enterobacteriaceae), J. Insect Physiol. 43 (1997) 1023–1029.

[46] A. Wiesner, P. Gotz, C. Weise, P. Kopacek, S. Losen, Isolated Apolipophorin III from Galleria mellonella Stimulates the Immune Reactions of This Insect, J. Insect Physiol. 43 (1997) 383–391.
[47] M. Oztug, D. Martinon, P.M. Weers, Characterization of the apoLp-III/LPS complex: insight into the mode of binding interaction, Biochemistry 51 (2012) 6220–6227.
[48] W.H.J. Beck, C.P. Adams, I.M. Biglang-awa, A.B. Patel, H. Vincent, E.J. Haas-Stapleton, P.M.M. Weers, Apolipoprotein A–I binding to anionic vesicles and lipopolysaccharides: role for lysine residues in antimicrobial properties, Biochim. Biophys. Acta Biomembr. 1828 (2013) 1503–1510.
[49] P.C.N. Rensen, M. van Oosten, E. Bilt, M. Eck, J. Kuiper, T.J.C. Berkel, Human recombinant apolipoprotein E redirects lipopolysaccharide from Kupffer cells to liver parenchymal cells in rats In vivo, J. Clin. Invest. 99 (1997) 2438–2445.
[50] E.S. Van Amersfoort, T.J.C. Van Berkel, J. Kuiper, Receptors, mediators, and mechanisms involved in bacterial sepsis and septic shock, Clin. Microbiol. Rev. 16 (2003) 379–414.
[51] M. Van Oosten, P.C.N. Rensen, E.S. Van Amersfoort, M. Van Eck, A.M. Van Dam, J.J. Breve, T. Vogel, A. Panet, T.J.C. Van Berkel, J. Kuiper, Apolipoprotein E protects against bacterial lipopolysaccharide-induced lethality. A new therapeutic approach to treat gram-negative sepsis, J. Biol. Chem. 276 (2001) 8820–8824.
[52] J. Xicohtencatl-Cortes, J. Mas-Oliva, R. Castillo, Phase transitions of phospholipid monolayers penetrated by apolipoproteins, J. Phys. Chem. B 108 (2004) 7307–7315.
[53] M. Luckey, Membrane structural biology, 1st ed. Cambridge University Press, Cambridge, 2008.
[54] M.A. Mitsche, D.M. Small, C-terminus of apolipoprotein A-I removes phospholipids from a triolein/phospholipids/water interface, but the N-terminus does not: a possible mechanism for nascent HDL assembly, Biophys. J. 101 (2011) 353–361.
[55] S.M. Storey, A.L. McIntosh, S. Senthivinayagam, K.C. Moon, B.P. Atshaves, The phospholipid monolayer associated with perilipin-enriched lipid droplets is a highly organized rigid membrane structure, Am. J. Physiol. Endocrinol. Metab. 301 (2011) E991–E1003.
[56] O. Domenech, J. Ignes-Mullol, M.T. Montero, J. Hernandez-Borrell, Unveiling a complex phase transition in monolayers of a phospholipid from the annular region of transmembrane proteins, J. Phys. Chem. B 111 (2007) 10946–10951.
[57] O. Domenech, F. Sanz, M.T. Montero, J. Hernandez-Borrell, Thermodynamic and structural study of the main phospholipid components comprising the mitochondrial inner membrane, Biochim. Biophys. Acta 1758 (2006) 213–221.
[58] P. Saulnier, F. Foussard, F. Boury, J.E. Proust, Structural properties of asymmetric mixed-chain phosphatidylethanolamine films, J. Colloid Interface Sci. 218 (1999) 40–46.
[59] C.P. Wan, M.H. Chiu, X. Wu, S.K. Lee, E.J. Prenner, P.M. Weers, Apolipoprotein-induced conversion of phosphatidylcholine bilayer vesicles into nanodisks, Biochim. Biophys. Acta 1808 (2011) 606–613.
[60] W.R. Schief, S.R. Dennis, W. Frey, V. Vogel, Light scattering microscopy from monolayers and nanoparticles at the air/water interface, Colloids Surf. A 171 (2000) 75–86.
[61] W.R. Schief, S.B. Hall, V.V. Vogel, Spatially patterned static roughness superimposed on thermal roughness in a condensed phospholipid monolayer, Phys. Rev. E Stat. Phys. Plasmas Fluids Relat. Interdiscip. Topics 62 (2000) 6831–6837.
[62] D. Fan, Y. Zheng, D. Yang, J. Wang, NMR solution structure and dynamics of an exchangeable apolipoprotein. *Locusta migratoria* apolipophorin III, J. Biol. Chem. 278 (2003) 21212–21220.
[63] J. Zimmerberg, M.M. Kozlov, How proteins produce cellular membrane curvature, Nat. Rev. Mol. Cell Biol. 7 (2006) 9–19.
[64] D. Marsh, Handbook of Lipid Bilayers, 2nd ed. CRC Press, Boca Raton, London, New York, 2013.